Biomaterials Science

ROYAL SOCIETY OF CHEMISTRY

PAPER

View Article Online
View Journal | View Issue

Cite this: *Biomater. Sci.*, 2025, **13**, 6652

misteINK: a protein nanocage-based ink with reversible, stimuli-responsive color shifts

Maika Yamashita, [a] Norifumi Kawakami, *[a] Ryoichi Arai, [b] Akihito Ikeda,[c] Toshio Moriya, [c] Toshiya Senda [c] and Kenji Miyamoto[a]

Dyes exhibiting polarity-dependent color changes, known as solvatochromism, have great potential for creating sensors, smart materials, and responsive coatings. However, full-range color shifts require a technique to disperse dyes across a wide range of solvent polarities, which remains a persistent challenge. For example, hydrophobic dyes often aggregate in water, preventing effective color shifts. Although surfactants can assist in dye dispersion, they can also prevent solvent molecules from accessing the dye. To address this, we used a 60-mer protein nanocage, TIP60, with a densely pyrene-modified interior surface. The modification did not induce protein denaturation, as monitored by small-angle X-ray scattering, and greatly increased the aqueous solubility of a hydrophobic solvatochromic dye, Nile Red (NR), while preserving its fluorescence. The NR-loaded solution appeared blue, reflecting the polar environment surrounding NR. Cryogenic electron microscopy suggested that the pyrenes interacted with each other to form a binding site for NR. This interaction also contributed to thermostability of TIP60 (65 °C to 86 °C) and stability against sodium dodecyl sulfate, as observed by electrophoresis experiments. When brushed onto plain copy paper, the NR-loaded nanocage appeared bluish-purple and shifted reversibly to purplish red upon heating, returning on cooling—presumably *via* nanocage dissociation and reassembly. The color change was also sensitive to humidity. We term this material "misteINK", a protein-based ink with reversible temperature- and humidity-dependent color changes. These findings demonstrate that a single-step interior modification enables the rational design of protein materials for tuning dye photophysics, providing a powerful strategy for designing protein-based functional materials.

Received 10th July 2025,
Accepted 5th October 2025

DOI: 10.1039/d5bm01052g

rsc.li/biomaterials-science

Introduction

Certain classes of dye molecules exhibit distinct colors depending on the solvent in which they are dissolved. This phenomenon, known as solvatochromism, primarily arises from differences in solvent polarity. Polar solvents stabilize the intramolecular charge-transfer (ICT) photoexcited state of solvatochromic dyes, which is formed by charge transfer from a donor group to an acceptor group. As a result, absorption and emission are red-shifted in more polar solvents.[1,2] Consequently, if dye molecules are dissolved in a variety of solvents with a wide range of polarities, large color changes should be possible. However, hydrophobic dyes often aggregate in water, preventing effective color changes.[3,4] Thus, a technique for dispersing dye molecules into layers with opposing properties could improve the color changes. Although hydrophobic dyes can be dispersed in aqueous media by using micelles and liposomes,[5–7] the dye molecules are often partitioned into hydrophobic domains formed by the hydrophobic moieties of amphiphilic molecules, thereby limiting the exposure of the dye to water. Consequently, the dyes show a color similar to that observed in organic solvents. Accordingly, a dye dispersion method that maintains accessibility to solvent molecules is essential for observing the color changes in solvatochromic molecules. In contrast to micelles, which spontaneously form flexible enclosed hydrophobic cores and sequester dyes away from water, structural rigidity in the dispersant is essential for keeping dyes accessible to the surrounding solvent. In addition, if dye molecules bind uniformly and specifically to identical binding sites, redesigning the binding sites could alter the solvent accessibility, resulting in further color changes.

Protein nanocages fulfill these criteria owing to their uniform structure and rigidity.[8–10] Based on these properties, protein nanocages have been widely studied as dispersants for hydrophobic molecules, including dyes, drugs, and food

[a]*Department of Bioscience and Informatics, Faculty of Science and Technology, Keio University, Yokohama, Kanagawa 223-8522, Japan.*
E-mail: norikawakami@bio.keio.ac.jp
[b]*Department of Applied Biology, Faculty of Textile Science and Technology and Institute for Biomedical Sciences, Shinshu University, Ueda, Nagano 386-8567, Japan*
[c]*Structural Biology Research Center, Institute of Materials Structure Science, High Energy Accelerator Research Organization (KEK), Oho, Tsukuba, Ibaraki 305-0801, Japan*

additives.[11–16] Proteins also allow site-specific structural design through genetic mutations and chemical modifications.[17–19] A variant of the E2 nanocage, derived from the E2 component of the pyruvate dehydrogenase multienzyme complex, has been used to encapsulate a hydrophobic drug molecule.[17] The hydrophilic amino acid residues on the interior surface were replaced with Phe residues. Encapsulation of the solvatochromic molecule, Nile Red (NR),[20,21] has also been demonstrated in protein nanocages. In engineered ferritin, phenylalanine clusters at twofold symmetry interfaces created an aromatic pocket that accommodated NR and supported bright emission, although wavelength shifts were not discussed.[22] In the artificial nanocage O3-33, the interior is filled with surfactants driven by electrostatic interactions between the negatively charged head group and the cationic amino acid residues introduced on the interior surface.[19] However, the fluorescence spectrum suggested that the encapsulated NR molecules were partitioned into the hydrophobic core of the micelles and were not exposed to water molecules.

Previously, we designed a protein nanocage, TIP60, composed of 60 identical fusion proteins.[23,24] The outer and inner diameters of TIP60 are 22 and 15 nm, respectively, and the molecular surface has 20 triangular pores with an inscribed circle 2.3 nm in diameter. Furthermore, a chemically modifiable cysteine residue can be introduced on the interior surface (S50C-TIP60). In our previous study, we modified the cysteine with the polycyclic aromatic molecule, pyrene, enabling the encapsulation of several aromatic fluorescent molecules, including NR, through the surface pores.[25] The absorption and fluorescence spectra of NR in modified TIP60 showed a similar pattern to that in the aqueous phase, suggesting that pyrene-modified TIP60 provides a chemical environment in which NR can bind while maintaining contact with water molecules. However, the amount of encapsulated NR was only 0.6 molecules per TIP60 nanocage.

In this study, to improve the encapsulation efficiency, we introduced an additional glycine-to-cysteine substitution at residue number 12 (G12C) into the S50C mutant, thereby increasing the number of modification sites to 120 per nanocage. The double mutant (DM)-TIP60 modified with pyrene achieved a 30-fold higher encapsulation capacity for NR compared with pyrene-modified S50C-TIP60. Cryogenic electron microscopy analysis suggested that the binding site of NR is formed by pyrenes arranged in a pentagram configuration. The pyrene modification improved the stability of the 60-mer structure. Finally, we demonstrated that DM-TIP60-encapsulated NR functions as a reversible, color-changing ink material on cellulose-based paper in response to heating and cooling.

Results and discussion

Design and modification of DM-TIP60

We initially determined the location of the second modification site in each monomer in addition to S50C, based on the 3D structure of TIP60 (PDB ID:7EQ9). The Ser50 residue was on the outer edge of the pentameric LSm domain (Fig. 1a, magenta sphere), with limited space available around the edge for a second modification site. The structure suggested that there might still be available space toward the central part of the LSm domain for pyrene modification. To minimize the effect on the original structure when introducing cysteine, Gly12 at the loop was selected as the second modification site (Fig. 1a, cyan sphere). We also used two single mutants (S50C-TIP60 and G12C-TIP60) for control experiments.

The mutants were modified with *N*-(1-pyrenyl)maleimide (Pyr-M) after expression and purification (Fig. 1b).[26] The modification was confirmed by fluorescence measurements because the pyrene group of Pyr-M only fluoresces after the maleimide group reacts with the thiol group.[27] The mixture of DM-TIP60 and Pyr-M showed typical pyrene emissions and an additional

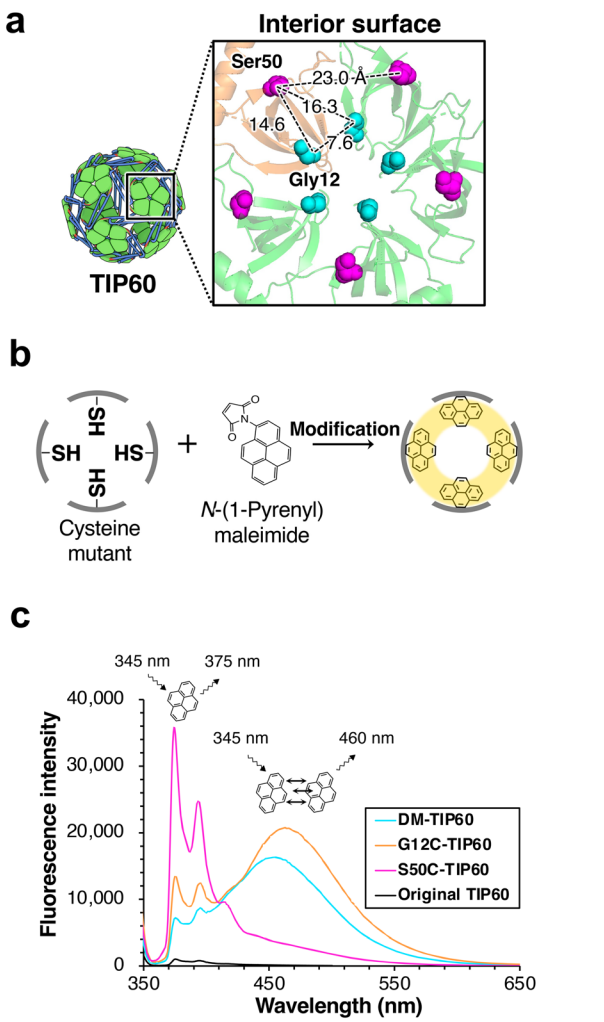

Fig. 1 (a) 3D structure of TIP60. Close-up view shows the interior surface of pentameric domain. One of the subunits is highlighted in orange. The Ser50 and Gly12 residues are shown as magenta and cyan, respectively. The values with dashed lines are distances. (b) Schematic of interior surface modification of TIP60 mutants with Pyr-M. (c) Emission spectra of TIP60 mutants modified with Pyr-M. The cysteine concentration was adjusted to 30 μM. All samples were excited at 345 nm.

longer-wavelength band around 460 nm, indicative of pyrene excimer formation (Fig. 1c, cyan).[28] A similar excimer band slightly shifted to a longer wavelength was observed for G12C-TIP60 (Fig. 1c, orange). In contrast, pyrene-modified S50C-TIP60 showed almost no excimer band (Fig. 1c, magenta). These data suggest that the pyrene molecules interacted with each other in DM-TIP60 and the G12C-TIP60 due to the proximity of the cysteine residues (Fig. 1a). Because the excimer formation prevented quantitative analysis of modification efficiency, the efficiency was estimated based on UV-vis absorbance measurements (see SI). For all mutants, the modification ratio was estimated to be around 75% (74.3%, 73.7%, and 76.8% for S50C-TIP60, G12C-TIP60, and DM-TIP60, respectively).

Encapsulation of NR

DM-TIP60 modified with Pyr-M was expected to have a higher encapsulation capacity for hydrophobic molecules than modified

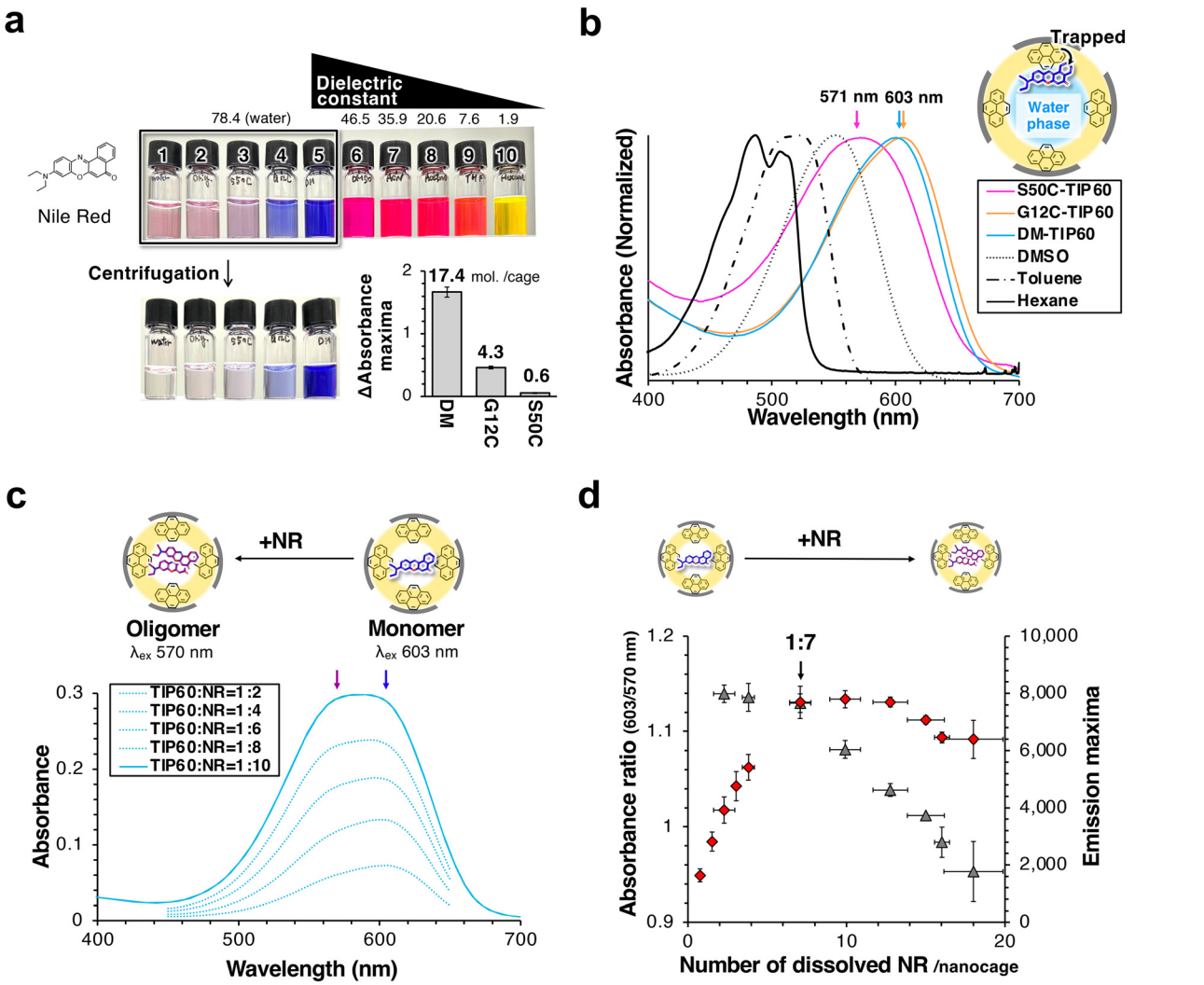

Fig. 2 (a) Photographs of 0.1 mM NR solutions in various solvents: (1) buffer comprising 20 mM Tris-HCl and 1 mM EDTA, adjusted to pH 7.4 (TE buffer), (2) 3 μM original TIP60 in TE buffer, (3) pyrene-modified S50C in TE buffer, (4) pyrene-modified G12C-TIP60 in TE buffer, (5) pyrene-modified DM-TIP60 in TE buffer, (6) DMSO, (7) acetonitrile, (8) acetone, (9) tetrahydrofuran, and (10) n-hexane. NR was dissolved in DMSO and added to the solvent at a final concentration of 0.1 mM. Photographs were taken 2 h after mixing (top), followed by centrifugation (bottom). Dielectric constants of the solvents at 25 °C were taken from ref. 29 and are indicated on the photographs. The bar graph displays the encapsulation amount of NR calculated from absorption spectra (see SI). (b) Normalized absorption spectra of solutions containing 5 μM NR and 3 μM of pyrene-modified DM-TIP60 (cyan), G12C-TIP60 (orange), and S50C-TIP60 (magenta). Black solid, dashed-dotted, and dotted lines show the NR absorption spectra in hexane, toluene, and DMSO, respectively. Absorption and emission wavelengths in various solvents are summarized in Table S1. (c) Absorption spectra of mixtures containing different ratios of modified DM-TIP60 and NR. The panel at the top of the spectra is a schematic of the proposed states of encapsulated NR. (d) Changes in the absorbance ratio at 603/570 nm (black, left axis) and the maximum fluorescence intensity (red, right axis) as a function of the number of NR molecules per nanocage for the modified DM-TIP60 solution with increasing NR concentration. Error bars denote the standard deviation of three independent experiments. Control experimental data for panels c and d using pyrene-modified S50C-TIP60 and G12C-TIP60 are summarized in Fig. S2c.

single mutants. To test this, the modified TIP60 variants were used to encapsulate the solvatochromic compound, NR. Each sample was mixed with excess NR and undissolved NR was removed by centrifugation. Although NR is generally yellow to red in hydrophobic solvents,[30] the mixture was bluish (Fig. 2a). This long-wavelength shift was observed in all three modified mutants, suggesting that encapsulated NR had contact with water molecules, which have a higher dielectric constant (a parameter reflecting solvent polarity) than organic solvents (Fig. 2b). A gradual increase in color intensity in the order of S50C, G12C, and DM-TIP60 was observed (Fig. 2a). The numbers of encapsulated NR were 0.6, 4.3, and 17.4 for S50C, G12C, and DM-TIP60, respectively, determined based on absorbance (Fig. 2a, bar graph). Thus, modified DM-TIP60 had a much greater encapsulation capacity than S50C and G12C-TIP60.

The spectra obtained from mixtures of modified DM-TIP60 and NR at various ratios revealed two peaks at 603 and 570 nm (Fig. 2c). Monomeric NR, which partially dissolves in aqueous solution, shows an absorbance at 593 nm.[30] Thus, the absorbance at 603 nm probably corresponded to monomeric NR in a polar environment. In contrast, the increase in absorbance at 570 nm probably indicated the formation of aggregates.[4,5] The absorbance ratio of 603 to 570 nm increased linearly up to an NR ratio of 7, remained constant until 12, and then decreased slightly (Fig. 2d, black). These results suggested that NR initially bound to DM-TIP60 as a monomer, and that above the binding capacity, excess NR formed aggregates at higher ratios. Aggregation formation was supported by fluorescence spectroscopy (Fig. 2d, red). At low concentrations, the fluorescence intensity increased linearly with a good fluorescence quantum yield of 0.08 (Fig. S2b), similar to quantum yields observed in protic solvents (*e.g.*, 0.12 in ethanol and 0.08 in methanol),[31] suggesting that the added NR was dissolved as the monomer. However, consistent with the absorption changes, once the NR-to-TIP60 ratio exceeded 7, no fluorescence intensity change was observed.

Structural analysis of pyrene-modified TIP60s

Structural changes in TIP60 mutants after chemical modification were analyzed using native polyacrylamide gel electrophoresis (native-PAGE) and small-angle X-ray scattering (SAXS). The band pattern and scattering curves after mutation and pyrene-modification were similar to those of the original TIP60 (Fig. 3a and b). The pair distance distribution ($P(r)$) of the mutants showed a right-shifted peak, indicative of a hollow spherical structure (Fig. 3c). *Ab initio* models (DAMMIF/DAMMIN) indicated that the modified TIP60 variants retained their original hollow structure (Fig. 3d). The radius of gyration

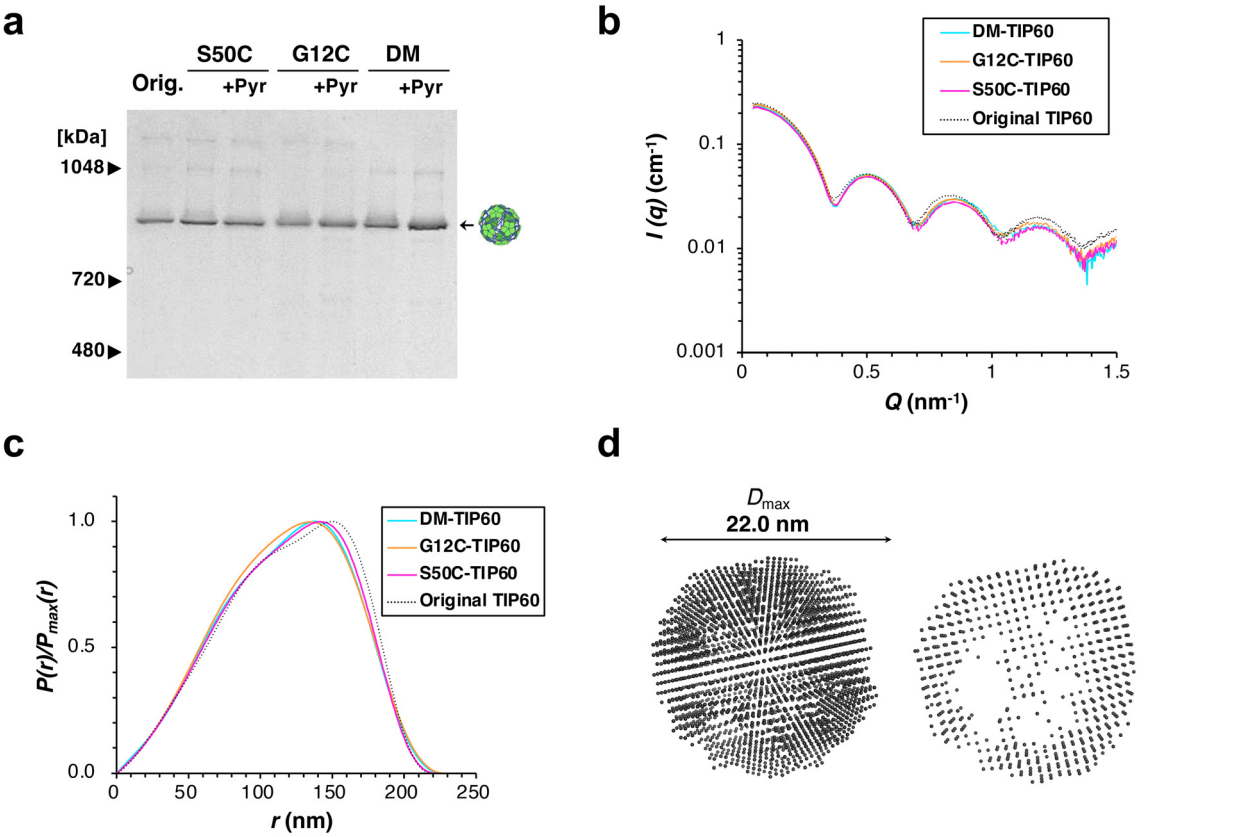

Fig. 3 (a) Native-PAGE results of the original TIP60 and unmodified (left lanes) and pyrene-modified TIP60 mutants (right lanes). (b) SAXS scattering curves of original TIP60 (black dotted line), pyrene-modified S50C-TIP60 (magenta), G12C-TIP60 (orange), and DM-TIP60 (cyan), respectively. (c) Pair-distance distribution ($P(r)$) calculated based on the data shown in panel b. (d) Dummy atom model of pyrene-modified DM-TIP60 (left panel) and a cross-sectional view (right panel).

(R_g) and the maximum particle dimension (D_{max}) were consistent with the values of the original TIP60 (Table S2). These results indicate that the overall structure remained essentially unchanged after modification with Pyr-M.

The three-dimensional (3D) structure of modified DM-TIP60 was analyzed by cryogenic electron microscopy (cryo-EM) in the presence of NR. Single-particle images were selected using two-dimensional (2D) and 3D classifications in RELION-4.0.2,[32] resulting in four distinct 3D classes (Fig. S3a). The reconstructed potential map of the dominant class, class 3 (22 050 particles), was refined to a resolution of 3.8 Å with icosahedral symmetry (Fig. 4a and Fig. S3a–d). The refined cryo-EM map and model structure are shown in Fig. S3e. The overall structures and the subunit structure were similar to those of the original TIP60 (PDB ID: 7EQ9) (backbone root-mean-square deviation (RMSD): 0.887 and 0.720 Å). An additional map was observed on the interior surface of the pentameric domain (Fig. 4a, right panel). The additional map was attributed to the pyrene groups; thus, we built an atomic model by fitting pyrene molecules into the map (Fig. 4b). The local resolution around the pyrene group models was slightly lower than that in the rigid pentamer region but higher than that in the C-terminal region of the dimeric domain (Fig. S4). The map was averaged with icosahedral symmetry and the heterogeneity of the pyrene modification may have affected the local resolution around the pyrene groups and the mean correlation coefficient between the model and corresponding experimental maps for the ligands (pyrene groups) (Table S3).

The pyrene groups had spatially close arrangements (Fig. 4c), suggesting that they interacted, consistent with the spectroscopic analysis (Fig. 1c). Pyrenes on the G12C residues (P1–P5) formed a sequentially stacked and tilted configuration (interfacial angle: ~50°), with a single pyrene on S50C almost equidistant (~7–9 Å) between the two pyrenes on G12C (*e.g.*, P1, P5, and P9). We designated the arrangement of these 10 pyrenes as a "pyrene pentagram".

The reconstructed potential map of the minor class, class 1 (10 097 particles), was refined to a resolution of 4.0 Å with icosahedral symmetry (Fig. S3a and S5). The averaged structure with a double-shell shape suggested that modified DM-TIP60 could incorporate molecules through hydrophobic interactions with the pyrene pentagrams.

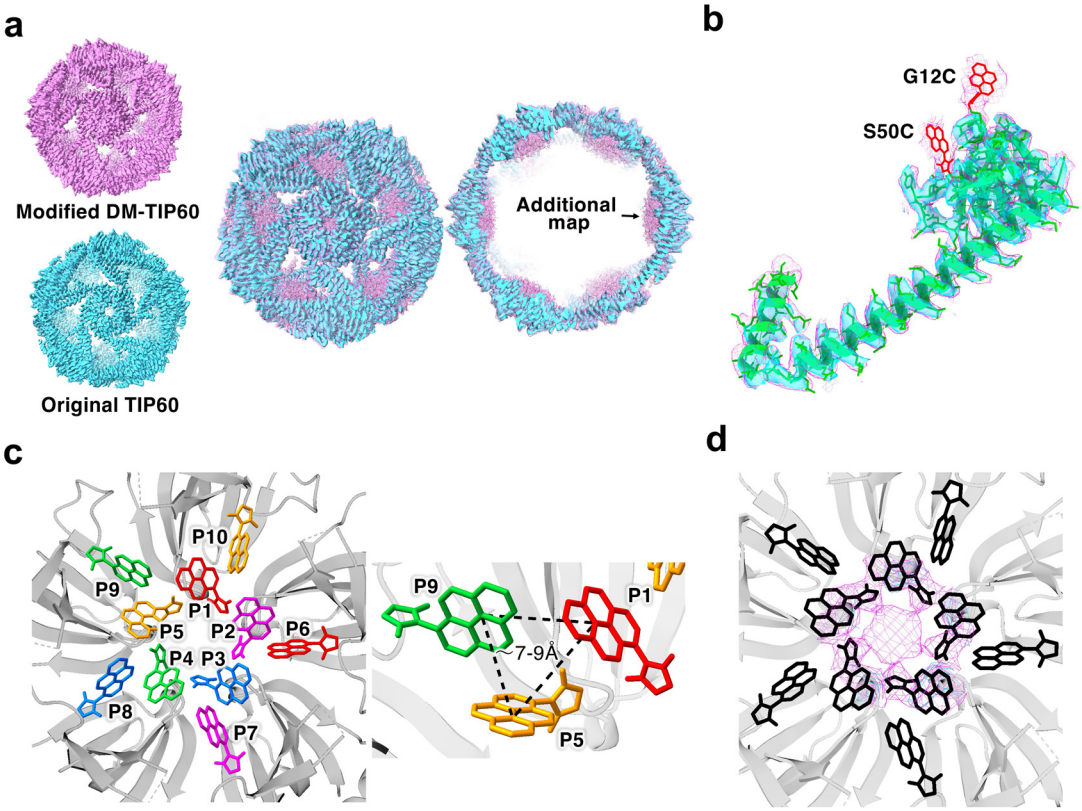

Fig. 4 (a) Cryo-EM potential map of original TIP60 (PDB: 7EQ9, EMDB: EMD-31256) (cyan) and pyrene-modified DM-TIP60 (PDB: 9UOL, EMDB: EMD-64381) (magenta). Full view of each map (left panel), superimposed view (center panel), and its cross-sectional view (right panel). (b) Refined model structure of a subunit of modified DM-TIP60 (green cartoon model with side chains) overlaid with partial potential maps extending 2.5 Å around the subunit (original TIP60, cyan surface; modified DM-TIP60, magenta mesh). The pyrene groups bound to G12C and S50C are shown as red sticks. (c) Pyrene pentagram observed on the pentameric subunits. Pyrene groups on the same monomer are highlighted in the same color. (d) Refined model structure of modified DM-TIP60 and potential maps representing a range of 8 Å from the pentamer center (original TIP60, cyan; modified DM-TIP60, magenta).

There was an additional map at the center of the pentamer cavity, even after placement and refinement of the pyrene groups (Fig. 4d and Fig. S6a). This map may correspond to the encapsulated NR, although the map resolution was not high enough to determine the binding site accurately. Possible binding models were constructed manually (Fig. S6b). This result explained the experimentally determined numbers of bound NR (17.4 mol per cage), which was higher than the number of pentamers of 12. The excess NR molecules were probably encapsulated by nonspecific hydrophobic interactions with the areas surrounding the pyrene pentagram. These results suggest that the pyrene pentagram provided an effective accommodation site for NR.

Evaluation of thermostability of pyrene-modified DM-TIP60

The 3D structure of modified DM-TIP60 suggested that pyrene groups on different fusion proteins may interact closely (Fig. 4c). We expected that these interactions among pyrenes would increase the thermostability of the nanocage. Modified DM-TIP60 exhibited a two-step dissociation pattern (Fig. 5a), although other TIP60 samples showed a single-step dissociation pattern. The melting temperatures estimated from the first and second dissociation processes of modified DM-TIP60 were 65 and 86 °C, respectively. The melting temperature of 65 °C was comparable to the melting points of other samples (69 °C). We assumed that this two-step dissociation was caused by the incomplete modification ratio of cysteine residues (76.8%). Fully modified pentamers can form pyrene pentagrams, whereas partially modified pentamers cannot. When a sufficient proportion of the pentamers in the 60-mer are fully modified and form the pyrene pentagrams, the 60-mer becomes stable. Sodium dodecyl sulfate (SDS)-PAGE analysis of modified DM-TIP60 showed bands at positions corresponding to the molecular weights of the pentamers and monomers (Fig. 5b), suggesting that only fully modified pentamers had a conformation that was resistant to thermal denaturation and SDS treatment.

We used size-exclusion chromatography (SEC)-multiangle light scattering (MALS) to measure the molecular weight of modified DM-TIP60 heated at 75 °C. Two peaks appeared, and the molecular weights were 1133 kDa (State 1) and 339 kDa (State 2) (Fig. 5c). The molecular weight of 1133 kDa was con-

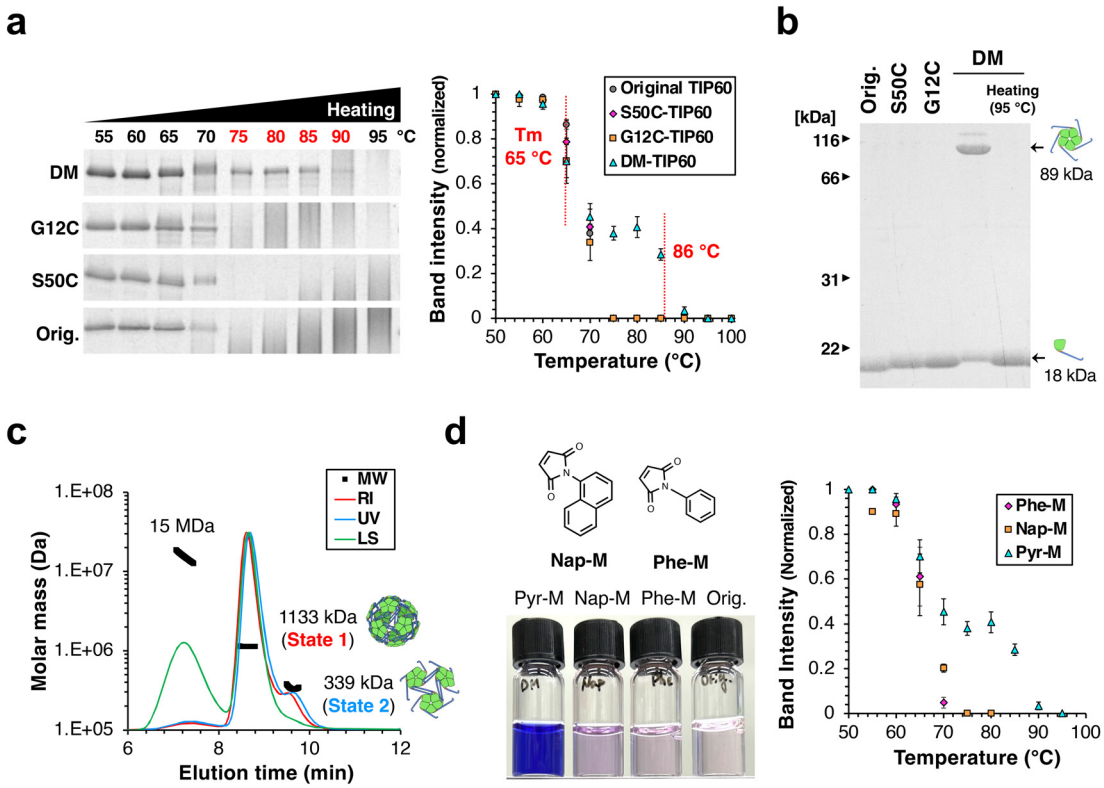

Fig. 5 (a) Native-PAGE analysis of heat-treated original TIP60 and pyrene-modified TIP60 mutants (left panel) and correlation between the heated temperature and the band intensities (right panel). Each sample was heated at 55–95 °C for 5 min in TE buffer. Two melting temperatures were determined by fitting logistic functions within specific temperature ranges (50–75 °C and 70–100 °C). (b) SDS-PAGE analysis for original TIP60 and pyrene-modified TIP60 mutants. All lanes are unheated unless otherwise indicated; the far-right lane shows modified DM-TIP60 heated at 95 °C for 5 min. (c) SEC-MALS analysis of modified DM-TIP60 heated at 75 °C for 5 min. Chromatogram traces are normalized to the monomer peak and offset for clarity. Each line shows the refractive index (RI) signal (red), UV absorbance signal (blue), and light scattering (LS) signal (green). Black squares represent the calculated molecular weight. (d) Analysis of DM-TIP60 modified with smaller aromatic molecules, Nap-M and Phe-M. Experimental conditions are identical to those in Fig. 2a and (a).

sistent with the theoretical molecular weight (1108 kDa) of pyrene-modified DM-TIP60. SAXS analysis of the State 1 fraction revealed oscillatory scattering typical of monodisperse large spherical particles, indicating that the cage structure was retained (Fig. S7a). The State 2 fraction with a molecular weight of 339 kDa was probably composed of a trimer of pentamers (277 kDa) or a tetramer of pentamers (369 kDa). In contrast, heat-treated original TIP60 did not form such partially stabilized structures (Fig. S7b). Accordingly, the pentamer-trimer and/or pentamer-tetramer may be stabilized by pyrene pentagrams unevenly distributed within the 60-mer.

In the control experiments, DM-TIP60 was modified with smaller aromatic molecules, *N*-(2-naphthyl)maleimide (Nap-M) and *N*-phenyl maleimide (Phe-M). These modified proteins exhibited neither improved nanocage thermostability nor effective NR encapsulation (Fig. 5d), probably because the sizes of Nap-M and Phe-M were insufficient to allow intermolecular interactions, emphasizing the critical role of pyrene-based aromatic interactions.

Application of NR-loaded TIP60 as protein-based ink (misteINK)

We examined the suitability of NR solubilized by modified DM-TIP60 as a protein-based ink material. The solution containing NR-loaded, pyrene-modified DM-TIP60 (NR-PyDM, see SI) was used to paint an illustration of TIP60 pentamers on paper (Fig. 6a). Dried NR-PyDM on paper was bluish-purple,

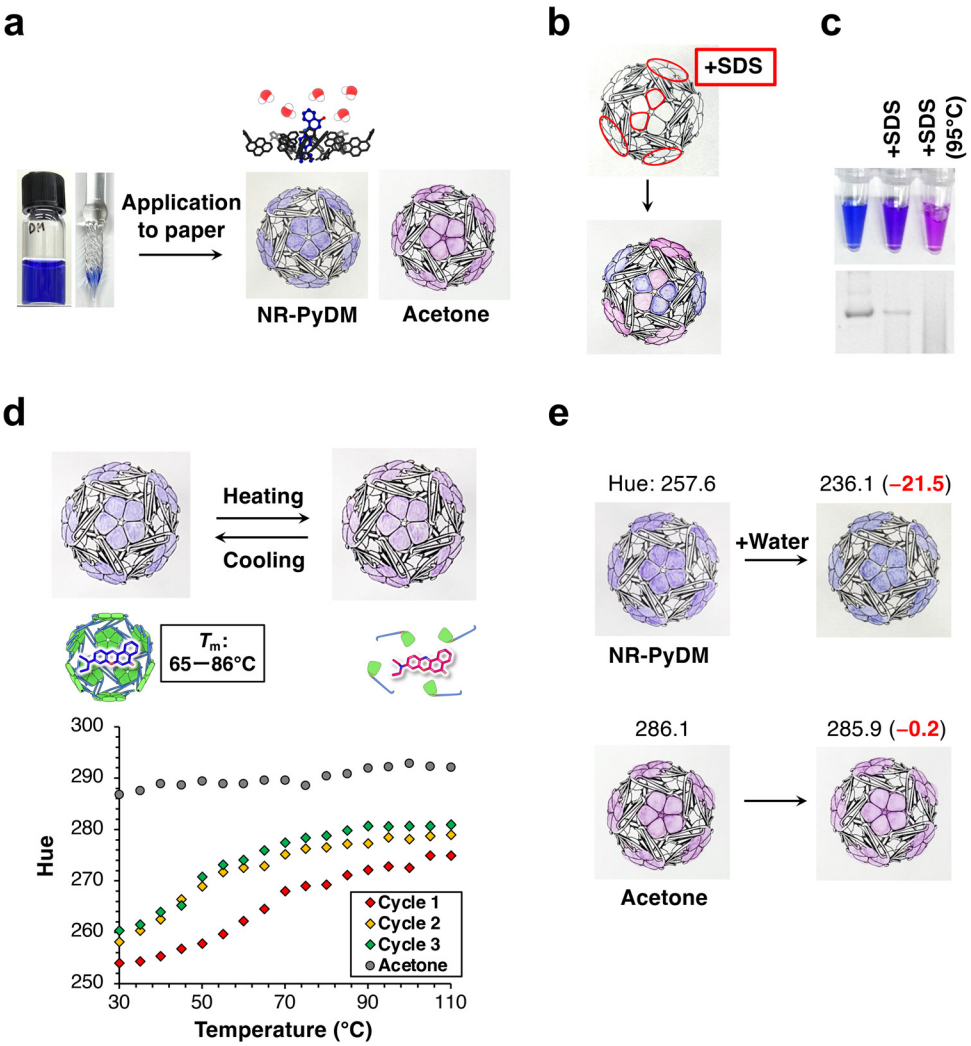

Fig. 6 (a) Photographs of NR-PyDM applied directly to paper using a glass pen. A schematic model of the encapsulated NR is show above the photograph, highlighting contact with water molecules. (b) Photographs of NR-PyDM applied to paper after an area was pre-treated with TE buffer containing 10% SDS and dried. (c) Photographs of NR-PyrDM solution (left), NR-PyrDM solution with 0.1% SDS (middle), and NR-PyrDM solution after heating at 95 °C for 5 min (right). The corresponding native-PAGE results are shown in the bottom panel. (d) Heat-responsive color transition of NR-PyDM on paper during hot plate heating. Representative photographs (top panel, before and after heating) and hue values measured at various temperatures (bottom panel). A schematic model showing the structural changes in pyrene-modified DM-TIP60 by heating is shown below the photograph. The full set of photographs used for the hue analysis is shown in Fig. S8a. (e) Photographs of NR-PyDM-painted paper before (top left) and after (top right) spraying with water. Corresponding control experiments with NR applied using acetone are shown in the bottom panels. Average hue values were measured in ImageJ, normalized to a 0°–360° scale, and are shown on each photograph.

whereas NR dissolved in acetone was pink (Fig. 6a, right panel), suggesting that NR remained encapsulated in the DM-TIP60 cavity by maintaining contact with water molecules even on paper. These results indicated that protein structure was important for the color change of NR. Then, we applied the NR-PyDM solution to paper pre-treated with SDS to induce nanocage denaturation, resulting in a pink color (Fig. 6b). A similar color change was observed when SDS was added directly to the solution (Fig. 6c), probably because NR transitioned to a non-polar environment by being released from DM-TIP60.

We investigated color changes associated with heat-induced protein disassembly. The color changed from bluish-purple to purplish red upon heating (Fig. 6d, top panel). Furthermore, the temperature-dependent color change visually appeared reversible. Analysis of color images based on hue values at each temperature demonstrated that the color change was reversible for at least three cycles (Fig. 6d, bottom panel), although a slight baseline increase was shown after the second cycle. In all cycles, the hue values stabilized at temperatures above 65 °C, matching the melting temperature of modified DM-TIP60. In contrast, NR applied using acetone showed only minor color changes owing to the weak thermochromic properties of NR (Fig. 6d, black).[20] These findings suggest that the color changes were associated with the dissociation and re-association of the 60-mer structure. In aqueous solution, however, no such reversible color change was observed due to the irreversible denaturation of TIP60 (Fig. S8b). Thus, the proteins on paper presumably do not undergo complete denaturation, likely because molecular mobility is restricted in the solid state. As a control experiment, a solutions containing the same weight concentration of bovine serum albumin (BSA) was used to dissolve NR, but it did not dissolve NR effectively and thus could not be used for comparison (Fig. S8c). We further observed an increase in the overall hue value after the second cycle of heat treatment. We hypothesize that the proteins on the paper immediately after application contained water molecules in excess of the equilibrium level. Thus, the initial heat treatment released the water molecules from NR. Upon cooling, NR was rehydrated under equilibrium conditions determined by the experimental humidity. This process may explain the baseline increase in hue values observed after the second cycle. To test the effect of hydration, we sprayed water onto NR-PyDM-painted paper. NR-PyDM turned blue, resembling its solution state, and reverted to bluish-purple upon drying (Fig. 6e). Heat treatment following hydration resulted in a hue increase similar to that in Fig. 6d (Fig. S8d, red), with a more distinct sigmoidal pattern. We repeated the rehydration experiment before heat treatment for an additional two cycles, and rehydration prevented the baseline increases (Fig. S8d, orange and green). The midpoint temperatures were 67, 73, and 85 °C for the first, second, and third cycles, respectively, as determined from the fitting curves. These values were between the two melting points of modified DM-TIP60 (65 and 86 °C, Fig. 5a), suggesting that the two-step disassembly of the nanocage was associated with the color change. Overall, these results indicate that the protein structure is essential for retaining water molecules around the bound NR. Inspired by the unique color change in response to local water content, we named this ink material "misteINK", derived from *mist* (humidity), pro*tein*, and *ink*.

Conclusions

We demonstrated that densely pyrene-modified DM-TIP60 dispersed the solvatochromic dye NR in a polar environment. The loading capacity reached 17.4 NR molecules per cage—approximately 30-fold higher than in our previous pyrene-modified S50C-TIP60. The well-ordered pyrene pentagram, unlikely to be formed by modified S50C alone, may enhance the loading capacity. Furthermore, this pentagram structure improved thermostability of TIP60. These results suggest that chemical modification remains a powerful approach for the functional design of proteins. Although computational approaches are becoming a standard tool, the structural and functional effects of non-natural chemical groups in proteins provide valuable insights for advancing future rational design strategies. We monitored the color change of NR on cellulose-based paper, presumably reflecting the dissociation and re-association of TIP60. Although the structural evaluation of TIP60 on solid phases remains insufficient, our findings suggested that the color change was primarily driven by changes in the local water content, which were influenced by the structural transitions of the nanocage. The protein created a dynamic microenvironment that retained water molecules around the encapsulated dye. This hydration-sensitive response allows our protein-based ink, misteINK, to function as a humidity-responsive optical material that could serve as a useful model for clarifying protein dynamics. We further anticipate that the pyrene pentagram can be extended to other planar solvatochromic dyes (*e.g.*, Prodan, Reichardt's Dye, Coumarin 153). Using such probes in combination could broaden both spectral windows and polarity readouts on paper-based systems, enabling multiplex sensing. Furthermore, this protein-based ink shows promise for applications in smart printing technologies and responsive biosensing systems. Integrating these findings with previous studies on TIP60, including gelation[33] and metal-responsive reassembly,[34] is expected to accelerate the development of multifunctional materials with diverse applications.

Author contributions

M. Y. and N. K. designed the study. M. Y. performed all experiments. R. A. supported SAXS measurements. R. A., A. I., T. M., and T. S. performed cryo-EM data collection and analysis. M. Y. and N. K. analyzed the data and interpreted the results. M. Y. and N. K. wrote the original manuscript. N. K. and K. M. edited and revised the manuscript. All authors reviewed and approved the final manuscript.

Conflicts of interest

There are no conflicts to declare.

Data availability

All data supporting the findings of this study are available within the article and its supplementary information (SI). Supplementary information is available. See DOI: https://doi.org/10.1039/d5bm01052g.

Raw data are available from the corresponding author upon reasonable request.

The cryo-electron microscopy (cryo-EM) map and the associated atomic model have been deposited in the Electron Microscopy Data Bank (EMDB) and the Protein Data Bank (PDB) under accession codes EMD-64381 and 9UOL, respectively.

Acknowledgements

The authors thank Dr Masato Kawasaki at KEK for managing the cryo-EM microscope and the staff of the Photon Factory (PF) for their help in SAXS experiments, which were performed at PF, KEK, under the approval of the PF program advisory committee (proposal number 2022G667).

This research was supported by the Research Support Project for Life Science and Drug Discovery (Basis for Supporting Innovative Drug Discovery and Life Science Research (BINDS)) from AMED under Grant Number JP24ama121001 (support number 6402).

This work was also supported by JSPS KAKENHI Grant Number JP24KJ1946 (Research Fellowship for Young Scientists) and JST SPRING Grant Number JPMJSP2123 to M. Y., JSPS KAKENHI Grant Number JP18K05324 to N. K., and JSPS KAKENHI Grant Numbers JP17KK0104, JP19H02522, and JP24K01267 to R. A.

References

1 A. S. Klymchenko, *Acc. Chem. Res.*, 2017, **50**, 366–375.
2 M. Homocianu, *Microchem. J.*, 2024, **198**, 110166.
3 F. Würthner, T. E. Kaiser and C. R. Saha-Möller, *Angew. Chem., Int. Ed.*, 2011, **50**, 3376–3410.
4 R. Varghese and H.-A. Wagenknecht, *Chem. – Eur. J.*, 2010, **16**, 9040–9046.
5 I. N. Kurniasih, H. Liang, P. C. Mohr, G. Khot, J. P. Rabe and A. Mohr, *Langmuir*, 2015, **31**, 2639–2648.
6 B. Trappmann, K. Ludwig, M. R. Radowski, A. Shukla, A. Mohr, H. Rehage, C. Böttcher and R. Haag, *J. Am. Chem. Soc.*, 2010, **132**, 11119–11124.
7 J. Sloniec, M. Schnurr, C. Witte, U. Resch-Genger, L. Schröder and A. Hennig, *Chem. – Eur. J.*, 2013, **19**, 3110–3118.
8 H. Chen, X. Tan, Y. Fu, H. Dai, H. Wang, G. Zhao and Y. Zhang, *Food Hydrocolloids*, 2021, **121**, 107004.
9 T. G. W. Edwardson, M. D. Levasseur, S. Tetter, A. Steinauer, M. Hori and D. Hilvert, *Chem. Rev.*, 2022, **122**, 9145–9197.
10 N. Song, J. Zhang, J. Zhai, J. Hong, C. Yuan and M. Liang, *Acc. Chem. Res.*, 2021, **54**, 3313–3325.
11 R. Yang, Y. Gao, Z. Zhou, P. Strappe and C. Blanchard, *RSC Adv.*, 2016, **6**, 35267–35279.
12 L. Chen, G. Bai, S. Yang, R. Yang, G. Zhao, C. Xu and W. Leung, *Food Res. Int.*, 2014, **62**, 1147–1153.
13 Z. Zhen, W. Tang, C. Guo, H. Chen, X. Lin, G. Liu, B. Fei, X. Chen, B. Xu and J. Xie, *ACS Nano*, 2013, **7**, 6988–6996.
14 L. Chen, G. Bai, R. Yang, J. Zang, T. Zhou and G. Zhao, *Food Chem.*, 2014, **149**, 307–312.
15 D. Luque, A. de la Escosura, J. Snijder, M. Brasch, R. J. Burnley, M. S. T. Koay, J. L. Carrascosa, G. J. L. Wuite, W. H. Roos, A. J. R. Heck, J. J. L. M. Cornelissen, T. Torres and J. R. Castón, *Chem. Sci.*, 2014, **5**, 575–581.
16 J. Mikkilä, E. Anaya-Plaza, V. Liljeström, J. Caston, T. Torres, A. de la Escosura and M. A. Kostiainen, *ACS Nano*, 2016, **10**, 1565–1571.
17 D. Ren, M. Dalmau, A. Randall, M. M. Shindel, P. Baldi and S. Wang, *Adv. Funct. Mater.*, 2012, **22**, 3170–3180.
18 Y. Azuma, D. L. V. Bader and D. Hilvert, *J. Am. Chem. Soc.*, 2018, **140**, 860–863.
19 T. G. W. Edwardson, S. Tetter and D. Hilvert, *Nat. Commun.*, 2020, **11**, 5410.
20 C. M. Golini, B. W. Williams and J. B. Foresman, *J. Fluoresc.*, 1998, **8**, 395–404.
21 V. Martinez and M. Henary, *Chem. – Eur. J.*, 2016, **22**, 13764–13782.
22 Y. Hishikawa, T. Suzuki, B. Maity, H. Noya, M. Yoshizawa, A. Asanuma, Y. Katagiri, S. Abe, S. Nagatoishi, K. Tsumoto and T. Ueno, *Adv. Sci.*, 2025, **12**, 2417030.
23 N. Kawakami, H. Kondo, Y. Matsuzawa, K. Hayasaka, E. Nasu, K. Sasahara, R. Arai and K. Miyamoto, *Angew. Chem., Int. Ed.*, 2018, **57**, 12400–12404.
24 J. Obata, N. Kawakami, A. Tsutsumi, E. Nasu, K. Miyamoto, M. Kikkawa and R. Arai, *Chem. Commun.*, 2021, **57**, 10226–10229.
25 M. Yamashita, N. Kawakami and K. Miyamoto, *ChemPlusChem*, 2023, **88**, e202200392.
26 E. Nasu, N. Kawakami, N. Ohara, K. Hayashi and K. Miyamoto, *Protein Expression Purif.*, 2023, **205**, 106232.
27 J. Guy, K. Caron, S. Dufresne, S. W. Michnick, W. G. Skene and J. W. Keillor, *J. Am. Chem. Soc.*, 2007, **129**, 11969–11977.
28 G. Bains, A. B. Patel and V. Narayanaswami, *Molecules*, 2011, **16**, 7909–7935.
29 C. Reichardt and T. Welton, Appendix A: Properties, Purification, and Use of Organic Solvents, in *Solvents and Solvent Effects in Organic Chemistry*, Wiley-VCH, Weinheim, 4th edn, 2011, pp. 549–586.

30 J. F. Deye, T. A. Berger and A. G. Anderson, *Anal. Chem.*, 1990, **62**, 615–622.
31 N. Ghoneim, *Spectrochim. Acta, Part A*, 2000, **56**, 1003–1010.
32 D. Kimanius, L. Dong, G. Sharov, T. Nakane and S. H. W. Scheres, *Biochem. J.*, 2021, **478**, 4169–4185.
33 E. Nasu, N. Kawakami, S. Takamura, A. Hotta, R. Arai and K. Miyamoto, *Biomacromolecules*, 2024, **25**, 2358–2366.
34 N. Ohara, N. Kawakami, R. Arai, N. Adachi, T. Moriya, M. Kawasaki and K. Miyamoto, *J. Am. Chem. Soc.*, 2023, **145**, 216–223.